

Binarized Convolutional Landmark Localizers for Human Pose Estimation and Face Alignment with Limited Resources

Adrian Bulat and Georgios Tzimiropoulos
 Computer Vision Laboratory, The University of Nottingham
 Nottingham, United Kingdom

{adrian.bulat, yorgos.tzimiropoulos}@nottingham.ac.uk

Abstract

This work is on landmark localization using binarized approximations of Convolutional Neural Networks (CNNs). Our goal is to design architectures that retain the groundbreaking performance of CNNs for landmark localization and at the same time are lightweight, compact and suitable for applications with limited computational resources. To this end, we make the following contributions: (a) we are the first to study the effect of neural network binarization on localization tasks, namely human pose estimation and face alignment. We exhaustively evaluate various design choices, identify performance bottlenecks, and more importantly propose multiple orthogonal ways to boost performance. (b) Based on our analysis, we propose a novel hierarchical, parallel and multi-scale residual block architecture that yields large performance improvement over the standard bottleneck block when having the same number of parameters, thus bridging the gap between the original network and its binarized counterpart. (c) We also show that the performance boost offered by the proposed architecture is not only observed for the case of binary networks but also generalizes for the case of real valued weights and activations. (d) We perform a large number of ablation studies that shed light on the properties and the performance of the proposed block. (e) We present results for experiments on the most challenging datasets for human pose estimation and face alignment, reporting in many cases state-of-the-art performance. Code can be download from <http://www.cs.nott.ac.uk/~psxab5/binary-cnn-landmarks/>

1. Introduction

Landmark localization is the problem of localizing a pre-defined set of fiducial points on objects of interest which can typically undergo non-rigid deformations like the human body or face. Very recently, work on landmark local-

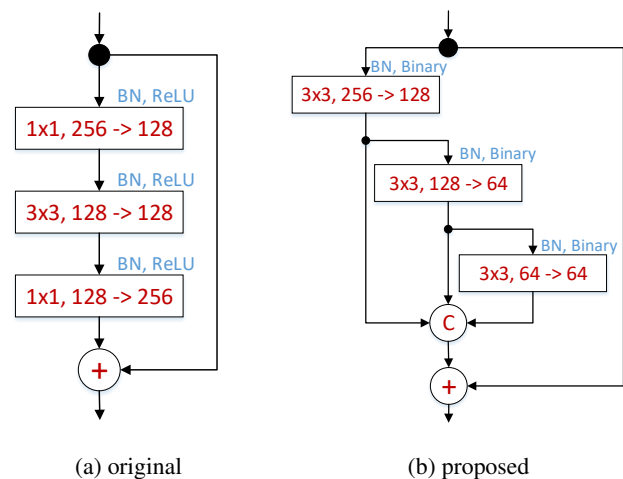


Figure 1: (a) The original bottleneck layer as proposed in [12]. (b) The proposed hierarchical parallel & multi-scale structure. Our block increases the receptive field size, improves gradient flow, is specifically designed to have a relatively low number of parameters, does not contain 1×1 convolutions, and in general is derived from the perspective of improving the performance and efficiency for binary networks. **Note:** a layer is depicted as a rectangular block containing: its filter size, the number of input and output channels; "C" - denotes concatenation and "+" an element-wise sum.

ization based on Convolutional Neural Networks (CNNs) has revolutionized landmark localization, demonstrating results of remarkable accuracy even on the most challenging datasets for human pose estimation [3, 23, 31] and face alignment [4]. However, training and more importantly deploying these methods is computationally expensive, requiring one or more high-end GPUs, while the learned models typically require hundreds of MBs, thus rendering these models completely unsuitable for real-time applications or

mobile devices. This work is on highly accurate and robust yet efficient and lightweight landmark localization using binarized CNNs.

Our work is inspired by very recent results on binarized versions of various CNN architectures for image classification [25, 10]. Contrary to these works, we are the first to study the effect of neural network binarization on fine-grained computer vision tasks like landmark localization. Similarly to [25, 10], we find that binarization results in performance drop, however to address this we opted to investigate and propose several architectural innovations which led to the introduction of a completely novel hierarchical, parallel and multi-scale residual block, as opposed to investigating ways to improve the binarization process as proposed in [25, 10].

In summary, **our contributions** are:

1. We are the first to study the effect of neural network binarization on state-of-the-art CNN architectures for the problem of localization, namely human pose estimation and face alignment. To this end, we exhaustively evaluate various design choices, and identify performance bottlenecks. More importantly, we describe multiple orthogonal ways to boost performance; see Subsections 4.2, 4.3 and 4.4
2. Based on our analysis, we propose a new hierarchical, parallel and multi-scale residual architecture described in Subsection 4.5 specifically designed to work well for the binary case. Our block results in large performance improvement over our baseline binary residual block of [12] (about 6-7% in absolute terms when the same number of parameters are used, see Subsection 5.1), bridging the performance gap between the original real-valued network and its binarized counterpart.
3. While our newly proposed block was developed with the goal of improving the performance of binary networks, we also show that the performance boost offered by the proposed architecture also generalizes for the case of real-valued networks (see Subsection 5.2).
4. We perform a large number of ablation studies that shed light on the properties and the performance of the proposed block (see Sections 7 and 5).
5. We present results for experiments on the most challenging datasets for human pose estimation and face alignment, reporting in many cases state-of-the-art performance (see Section 7)

2. Closely Related Work

This section reviews related work on network quantization (binarization) and architecture design, as well as gives

a quick overview of the state-of-the-art on human pose estimation and face alignment.

Network quantization. Previous work [13] suggests that high precision parameters are not essential for obtaining top results for image classification. In light of this, [8, 20] propose 16-bit and 8-bit quantization, showing negligible drop of performance on a few small datasets [19]. Zhou *et al.* propose a 1-2-6 bit quantization technique which allocates different numbers of bits for the network parameters, activations and gradients.

Note that the extreme case of the quantization (binarization) was long considered to be impractical due to the destructive property of such a representation [8]. However, recently Soudry *et al.* [27] showed this not to be the case and that by quantizing to $\{-1, 1\}$ good results can be actually obtained. Courbariaux *et al.* [9] introduce a new technique for training CNNs that makes use of binary weights for both forward and backward passes, however, the real parameters are still required during training. The work of [10] goes one step further and binarize both the parameters and the activation function. This case is of special interest since multiplications can be replaced with elementary binary operations [10]. By estimating the binary weights with the help of a scaling factor, computed as the average of absolute weight values, [25] is the first work to report good results on a large data set (ImageNet). Notably, our method makes use of the recent findings from [25] and [10] using the same way of quantizing the weights as well as replacing the multiplications with bit-wise *xor* operations.

Our method differs from all aforementioned works in two key respects: (a) instead of focusing on image classification, we are the first to study neural network binarization in the context of a fine-grained computer vision task namely landmark localization (human pose estimation and facial alignment) by predicting a dense output (heatmaps) in a fully convolutional manner, and (b) instead of enhancing the results by improving the quantization method, we follow a completely different path, by enhancing the performance via proposing a novel architectural design for a hierarchical, parallel and multi-scale residual block.

Block architecture design. The proposed method uses a residual-based architecture and hence the starting point of our work is the *bottleneck* block described in [11, 12]. More recently, [32] explores the idea of increasing the cardinality of the residual block by splitting it into a series of c parallel (and much smaller so that the number of parameters remains roughly the same) sub-blocks with the same topology which behave as an ensemble (see Figure 2a). Beyond bottleneck layers, Szegedy *et al.* [28] explores various ways of lowering the number of parameters by simply factorizing convolutional layers with large filters in smaller ones (see Figure 2b).

Our method is different from the aforementioned archi-

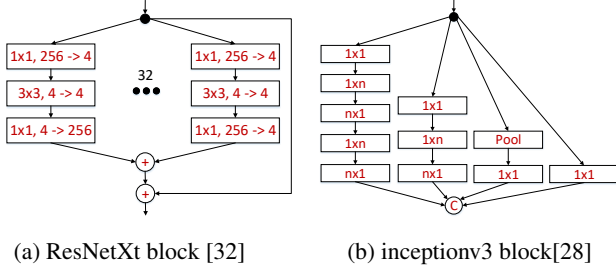


Figure 2: Block structure for (a) ResNetXt [32] and (b) Inception-v3 [28] networks. **Note:** a layer is depicted as a rectangular block containing: its filter size, the number of input and output channels; "C" - denotes concatenation and "+" an element-wise sum.

structures in the following ways (see also Fig. 1b): we create a hierarchical, parallel and multi-scale structure that (a) increases the receptive field size inside the block and (b) improves gradient flow, (c) our block structure is specifically designed to have a relatively low number of parameters, (d) our block does not contain 1x1 convolutions, and (e) our block is derived from the perspective of improving the performance and efficiency for binary networks.

Network architecture design. Our target was not to propose a new network architecture for landmark localization; hence we opted to use the state-of-the-art *Hour-Glass* (HG) network of [23] which makes use of the bottleneck block of [11]. Because we are interested in efficiency, all of our experiments are conducted using a single network i.e. we do not use stacking as in [23]. We used as a baseline the binary HG obtained by directly quantizing it using [25]. As Table 1) shows, there is a significant performance gap between the binary and the real valued HG. We bridge this performance gap by replacing the bottleneck block used in the original HG with the proposed hierarchical, parallel and multi-scale block.

Human Pose Estimation. Recent work has shown that CNNs produce remarkable results for the task of human pose estimation [30, 29, 24, 14, 3, 23, 31]. While achieving top performance, the above methods are computationally demanding, requiring at least one high-end GPU. In contrast, our method uses binary weights and activations for our network and as such is intended to run in real-time on systems with limited resources (e.g. smartphones, FPGAs).

Face alignment. Current state-of-the-art for large pose 2D and 3D face alignment is also based on CNNs [17, 2, 4]; however, these methods are also computationally demanding. Our network produces state-of-the-art results for this task, yet it is designed to run on devices with limited resources.

3. Background

This section introduces the residual block of [11, 12] and the *Hour of Glass* (HG) network of [23] (the residual block is the main building block of HG). Our baseline in this paper is a binarized version of HG (see section 4.1).

Residual blocks, as described in [11, 12], can be represented as follows:

$$\mathbf{x}_{l+1} = \mathbf{x}_l + \mathcal{F}(\mathbf{x}_l, \mathcal{W}_l), \quad (1)$$

where \mathbf{x}_{l+1} and \mathbf{x}_l are the input and outputs of the l -th block, \mathcal{F} is a residual function and \mathcal{W}_l denotes the unit parameters.

The ResNet consists of two type of blocks: *basic* and *bottleneck*. Of particular interest in this work is only the latter one which was designed to reduce the number of parameters and keep the network memory footprint under control. We use the "pre-activation" version of [12], in which batch normalization [15] and the activation function precede the convolutional layer. This block is shown in Fig. 1a. Note that we used the version of bottleneck defined in [23] the middle layer of which has 128 channels (vs 64 used in [12]).

The residual block is the main building block of HG which is a state-of-the-art architecture for landmark localization that predicts a set of heatmaps (one for each landmark) in a fully convolutional fashion. The HG network is an extension of [21] allowing however for a more symmetric top-down and bottom-up processing. See Fig. 3 for an overview of HG and [23] for more details.

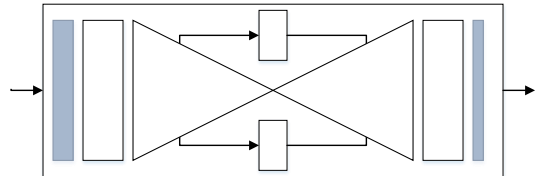


Figure 3: The *Hour-Glass* (HG) architecture. Following [25], the first and last layers (blue colour) are left real while all the remaining layers are binarized.

4. Method

In this section, we describe the proposed binary hierarchical, parallel and multi-scale block of Fig. 8e. The proposed block is an amalgamation of many ideas the goal of which is to overcome the performance drop of the standard residual block when binarized within the HG network. The section is organized as follows:

- We start by analyzing the performance of the binarized HG in Subsection 4.1 which provides the motivation as well as the baseline for our method.

- Then, we propose a series of architectural innovations in Subsections 4.2, 4.3, 4.4 and 4.5 each of which is evaluated and compared against the binarized residual block of Subsection 4.1. The proposed architectures are shown in Fig. 8b, 8c, and 8d.
- Finally, by combining ideas from these architectures, we propose the binary hierarchical, parallel and multi-scale block of Fig. 1b (for convenience also shown in Fig. 8e). Note that the proposed block is not a trivial combination of the previously described architectures but a completely new structure.

We note that all results for this section were generated for the task of human pose estimation by training the networks on the MPII [1] training set and evaluating on the MPII [1] validation set (this is the standard validation set used by many authors, see [3, 23]).

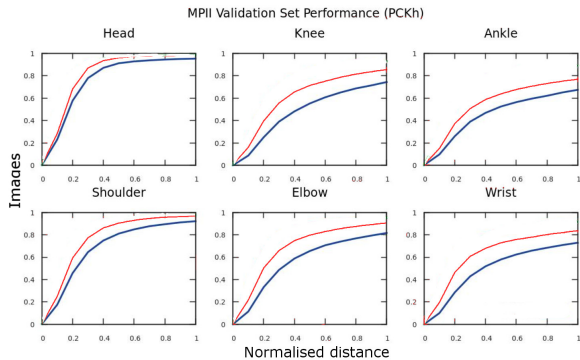


Figure 4: Cumulative error curves on MPII validation set for real-valued (red) and binary (blue) bottleneck blocks within the HG network.

4.1. Binarized HG

We start from the original HG network and quantize it during both forward and backward pass in a similar fashion to [25]. The binarization is accomplished using:

$$I * W \approx (\text{sign}(I) \otimes \text{sign}(W)) * \alpha, \quad (2)$$

where I is the input tensor, W represents the layer weights and α is a scaling factor. \otimes denotes the binary convolution operation which can be efficiently implemented with XNOR. Following [25], the first and last layers of the network are left real while all the remaining layers are binarized. We believe this to be crucial, especially for the very last layer where higher precision is required for producing a dense output (heatmaps). Note that these layers' account for less than 0.01% of the total number of parameters.

The performance of the original (real-valued) and the binarized bottleneck blocks within the HG network for the task of human pose estimation on MPII validation set can be seen in Table 1. We may observe that binarization results in significant performance drop. To further investigate this, we plot the cumulative error curves for each part separately in Fig. 4. As we may observe, for almost all parts, there is a large difference in performance across the whole spectrum of the landmark error (x-axis) which clearly indicates that the binary network has significant less representational power. Some failure cases are shown in Fig. 5 illustrating that the binary network was not able to learn some difficult poses. We address this with a better architecture as detailed in the next 4 Subsections.

Layer type	No. parameters	PCKh
Bottleneck (real)	3.5M	76.5%
Bottleneck (binary)	3.5M	67.2%

Table 1: PCKh error on MPII dataset for real-valued (red) and binary (blue) bottleneck blocks within the HG network.



Figure 5: Examples of failure cases for the binarized HG (first row). The second row shows the predictions of the equivalent real-valued HG. Notice that the binary HG misses certain range of poses while having similar accuracy for the correct parts.

4.2. On the Width of Residual Blocks

The original bottleneck block of Fig. 8a is composed of 3 convolutional layers of filter size 1×1 , 3×3 and 1×1 , with the first layer having the role of limiting the width (i.e. the number of channels) of the second layer, thus greatly reducing the number of parameters inside the module. However, it is unclear whether the idea of having a bottleneck structure will be also successful for the binary case, too. Due to the limited representational power of the binary layers, greatly reducing the number of channels might reduce the amount of information that can be passed from one layer to another, leading to lower performance.

To investigate this, we modify the bottleneck block by increasing the number of channels in the *thin* 3×3 layer from 128 to 256. By doing so, we match the number of channels from the first and last layer, effectively removing the “bottleneck”. This in turn increases the amount of information that can be passed from one block to another. The resulting **wider** block is illustrated in Fig. 8b. Here, “wider”¹ refers to the increased number of channels over the initial *thin* layer.

As Table 2 illustrates, while this improves performance against the baseline, it also raises the memory requirements. **Conclusion:** Widening the *thin* layer offers tangible performance improvement, however at a high computational cost.

4.3. On Multi-Scale Filtering

Recent studies have shown that small filters are both effective and efficient [26, 28] with the final model being solely made up by a combination of convolutional layers with 3×3 and/or 1×1 filters [11, 12, 26]. For the case of real-valued networks, a high variety of kernels can be learned. However, for the binary case, the number of possible unique convolutional kernels is limited to 2^k states only, where k represents the size of the filter. Examples of such 3×3 learned filters are illustrated in Fig. 6.

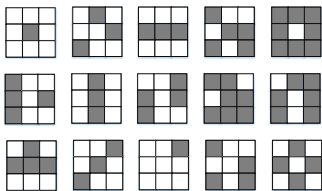


Figure 6: Examples of 3×3 filters learned by a convolutional layer.

In order to address the limited representation power of 3×3 filters for the binary case, we largely depart from the block of Fig. 8b by proposing the multi-scale structure depicted in Fig. 8c. Note that we implement our multi-scale approach using both larger filter sizes and max-pooling, which greatly increase the effective receptive field within the block. Also, because our goal is to analyze the impact of a multi-scale approach alone, we intentionally keep the number of parameters to a similar level to that of the original/baseline bottleneck block of Fig. 8a. To this end, we avoid a leap in the number of parameters, by (a) decomposing the 5×5 filters into two layers of 3×3 filters, and (b)

¹The term wider here strictly refers to a “moderate” increase in the number of channels in the middle layer (up to 256), effectively removing the “bottleneck”. Except for the naming there is no other resemblance with the work of [34] which performs a study of wide vs deep, using a different building block alongside a much higher number of channels (up to 2048) and without any form of quantization. A similar study falls outside the scope of our work.

by preserving the presence of *thin* layer(s) in the middle of the block.

Given these restrictions and the above-mentioned ideas, we split the input into two branches. The first (left) branch works at the same scale as the original bottleneck of Fig. 8a but has a 1×1 layer that projects the 256 channels into 64 (instead of 128) before going to the 3×3 one. The second (right) branch performs a multi-scale analysis by firstly passing the input through a max-pooling layer and then creating two branches, one using a 3×3 filter and a second one using a 5×5 decomposed into two 3×3 . By concatenating the outputs of these two sub-branches, we obtain the remaining 64 channels (out of the 128 of the original bottleneck block). Finally, the two main branches are concatenated adding up to 128 channels, which are again back-projected to 256 with the help of a convolutional layer with 1×1 filters.

The accuracy of the proposed structure can be found in Table 2. We can observe a healthy performance improvement at little additional cost and similar computational requirements to the original bottleneck of Fig. 8a.

Conclusion: When designing binarized networks, multi-scale filters should be preferred.

4.4. On 1×1 Convolutions

In the previously proposed block of Fig. 8c, we opted to avoid an increase in the number of parameters, by retaining the two convolutional layers with 1×1 filters. In this Subsection, by relaxing this restriction, we analyze the influence of 1×1 filters on the overall network performance.

In particular, we remove all convolutional layers with 1×1 filters from the multi-scale block of Fig. 8c, leading to the structure of Fig. 8d. Our motivation to remove 1×1 convolutions for the binary case is the following: because 1×1 filters are limited to two states only (either 1 or -1) they have a very limited learning power. Due to their nature, they behave as simple filters deciding when a certain value should be passed or not. In practice, this allows the input to pass through the layer with little modifications, sometimes actually blocking “good features” and hurting the overall performance by a noticeable amount. This is particular problematic for the task of landmark localization, where a high level of detail is required for successful localization. Examples of this problem are shown in Fig. 7.

Results are reported in Table 2. We can observe, that by removing 1×1 convolutions, performance over the baseline is increased by more than 8%. Even more interestingly, the newly introduced module outperforms the variant described in Subsection 4.2, while having less parameters, which clearly shows that the presence of 1×1 filters is limiting the performance of binarized CNNs.

Conclusion: The usage of 1×1 convolutional filters on binarized CNNs has a detrimental effect on performance and

should be avoided.

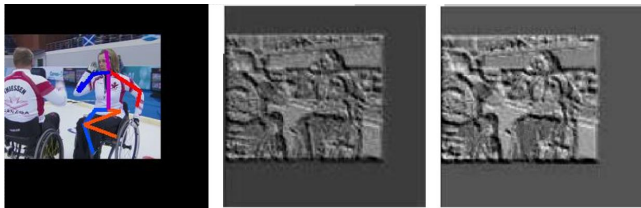


Figure 7: Examples of features before and after an 1×1 convolutional layer. Often the features are copied over with little modifications, usually consisting in the details’ removal. The contrast was altered for better visualization.

4.5. On Hierarchical, Parallel & Multi-Scale Filtering

Binary networks are even more sensitive to the problem of fading gradients [10, 25], and for our network we found that the gradients are up to 10 times smaller than those corresponding to its real-valued counterpart. To alleviate this, we design a new module which has the form of a hierarchical, parallel multi-scale structure allowing, for each resolution, the gradients to have 2 different paths to follow, the shortest of them being always 1. The proposed block is depicted in Fig. 8e. Note that, in addition to better gradient flow, our design encompasses all the findings from the previous Subsections: (a) no convolutional layers with 1×1 filters should be used, (b) the entire block should preserve its width as much as possible (avoiding large drops in the number of channels), and (c) multi-scale filters should be used.

Contrary to the blocks described in Subsections 4.2 - 4.4, where the gradients may need to pass through two more layers before reaching the output of the block, in the newly proposed module, each convolutional layer has a direct path that links it to the output, so that at any given time and for all the layers within the module the shortest possible path is equal to 1. The presence of a hierarchical structure inside the module efficiently accommodates larger filters (up to 7×7), decomposed into convolutional layers with 3×3 filters. Furthermore, our design avoids the usage of an element-wise summation layer as for example in [32], further improving the gradient flow and keeping the complexity under control.

As we can see in Table 2, the proposed block matches and even outperforms the block proposed in section 4.3 having far less parameters.

Conclusion: Good gradient flow and hierarchical multi-scale filtering are crucial for high performance without excessive increase in the parameters of the binarized network.

Block type	# params	PCKh
Bottleneck (original) (Fig. 8a)	3.5M	67.2%
<u>Wider (Fig. 8b)</u>	11.3M	70.7%
<u>Multi-Scale (MS) (Fig. 8c)</u>	4.0M	69.3%
<u>MS without 1×1 filters (Fig. 8d)</u>	9.3M	75.5%
<u>Hierarchical, Parallel & MS</u> (Ours, Final) (Fig. 8e)	6.2M	76%

Table 2: PCKh-based comparison of different blocks on MPII validation set. All underlined blocks are proposed in this paper. # params refers to the number of parameters of the whole network.

5. Proposed vs Bottleneck

This section provides some of the most important experimental results of this work: in particular we attempt to make a fair comparison between the performance of the proposed block (**(Ours, Final)** (Fig. 8e)) against that of the original bottleneck module (Fig. 8a) by taking two important factors into account:

- For the sake of a fair comparison, both blocks should have the same number of parameters. Notice that the proposed block of Fig. 8e has about 6M parameters while the original bottleneck Fig. 8a about 3.5M.
- The two blocks should be compared for the case of binary but also real-valued networks.

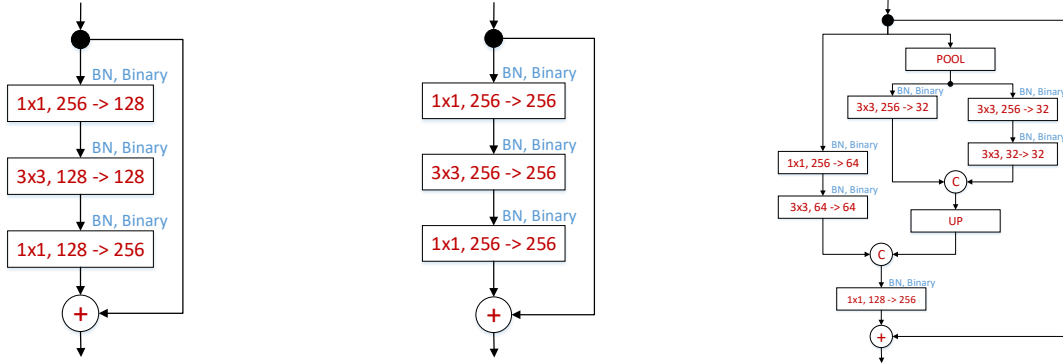
With this in mind, in the following Subsections, we present results that show:

- The proposed block largely outperforms a bottleneck with the same number of parameters for the binary case.
- The proposed block also outperforms a bottleneck with the same number of parameters for the real case but in this case the performance difference is smaller.

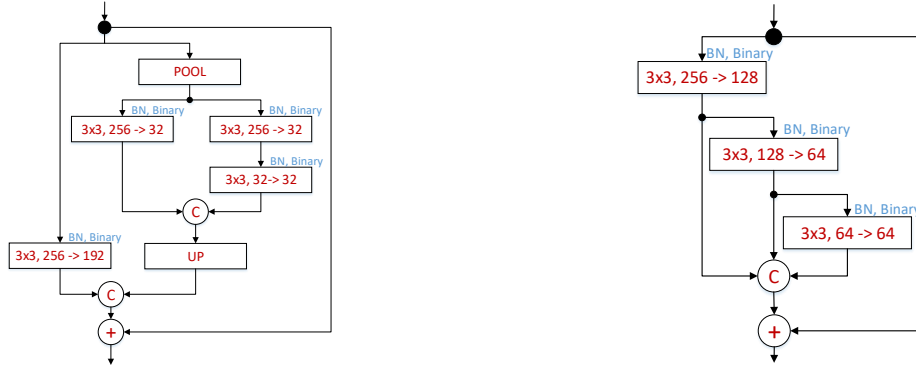
We conclude that, for the real case, increasing the number of parameters (in particular the width of the network) results in increase in performance; however this is not the case for binary networks where a tailored design as the one proposed in this work is needed.

5.1. Binary

To match the number of parameters between the proposed and bottleneck block, we follow two paths. Firstly, we increase the number of parameters of the bottleneck: (a) a first way to do this is to make the block wider as described in section 4.2. Note that in order to keep the number or input-output channels equal to 256, the resulting block of



(a) The **Original Bottleneck** block with pre-activation, as defined in [12]. Its binarized version is described in section 4.1. (b) The **Wider** version of (a) produced by increasing the number of filters in the convolutional layer. See also Subsection 4.2. (c) Largely departing from (b), this block consists of **Multi-Scale (MS)** filters for analyzing the input at multiple scales. See also Subsection 4.3.



(d) A variant of the MS block introduced in (c) after removing all convolutional layers with 1×1 filters (**MS Without 1×1 filters**). See also Subsection 4.3. (e) The proposed **Hierarchical, Parallel & MS** (denoted in the paper as **Ours, final**) block incorporates all ideas from (b), (c) and (d) with an improved gradient flow. The module is analyzed in Subsection 4.5

Figure 8: Different types of blocks described and evaluated. Our best performing block is shown in figure (e). A layer is depicted as a rectangular block containing: its filter size, number of input channels and the number of output channels). "C" - denotes concatenation operation and "+" an element-wise sum.

Fig. 8b has a far higher number of parameters than the proposed block. Despite this high increase in the number of parameters, the performance gain is only moderate (see section 4.2 and Table 3). (b) Because we found that the 1×1 convolutional layers have detrimental effect to the performance of the Multi-Scale block of Fig. 8c, we opted to remove them from the bottleneck block too. To this end, we modified the Wider module by (a) removing the 1×1 convolutions and (b) halving the number of parameters in order to match the number of parameters of the proposed block. The results in Table 4 clearly show that this modification is helpful but far from being close to the performance achieved by the proposed block.

Secondly, we decrease the number of parameters in the proposed block to match the number of parameters of the

original bottleneck. To this end, we reduced the number of input-output channels of the proposed block from 256 to 192 so that the number of channels in the first layer are modified from $[256 \rightarrow 128, 3 \times 3]$ to $[192 \rightarrow 96, 3 \times 3]$, in the second layer from $[128 \rightarrow 64, 3 \times 3]$ to $[96 \rightarrow 48, 3 \times 3]$ and in the third layer from $[64 \rightarrow 64, 3 \times 3]$ to $[48 \rightarrow 48, 3 \times 3]$. Notice, that even in this case, the proposed binarized module outperforms the original bottleneck block by more than 5% (in absolute terms) while both have very similar number of parameters (see Table 3).

Overall, our results clearly illustrate the need for a new design as proposed in Section 4.5 incorporating all ideas from Sections 4.2- 4.4.

Layer type	# parameters	PCKh
Bottleneck (Original) (Fig. 8a)	3.5M	67.2%
Wider (Fig. 8b)	11.3M	70.7%
Bottleneck (wider) + no 1×1	5.8M	69.5%
(Ours, Final) (Fig. 8e)	6.2M	76%

Table 3: PCKh-based performance on MPII validation set for binary blocks: the number of parameters of the original bottleneck are increased to match the number of parameters of the proposed block. This firstly gives rise to the Wider block and its variant without the 1×1 Convolutions. Observe that our block largely outperforms both of them.

Layer type	# parameters	PCKh
Bottleneck (original)	3.5M	67.2%
(Ours, Final) (Fig. 8e)	4.0M	72.7%

Table 4: PCKh-based performance on MPII validation set for binary blocks: the number of parameters of the proposed block are decreased to match the number of parameters of the original bottleneck. Observe that our block largely outperforms the original bottleneck.

5.2. Real

While the proposed block was derived from a binary perspective, Table 5 shows that a significant performance gain is also observed for the case of real-valued networks. In order to quantify this performance improvement and to allow for a fair comparison, we increase the number of channels inside the original bottleneck block so that both networks have the same depth and a similar number of parameters. Even in this case, our block outperforms the original block although the gain is smaller than that observed for the binary case. We conclude that for real-valued networks performance increase can be more easily obtained by simply increasing the number of network parameters, but for the binary case a better design is needed as proposed in this work.

Layer type	# parameters	PCKh
Bottleneck (wider)	7.0M	83.1%
(Ours, Final) (Fig. 8e)	6.2M	85.5%

Table 5: PCKh-based performance on MPII validation set for the real-valued version of the proposed block. Our block is compared with a wider version of the original bottleneck so that both blocks have a similar number of parameters.

6. Ablation studies

In this section, we further present a series of other architectural variations and their effect on the performance of our binary networks for the task of human pose estimation. All reported results are obtained using our **hierarchical, parallel & multi-scale** block of Fig. 8e coined **Ours, Final**. We focus on the effect of augmentation and different loss which are novel experiments not reported in [25], and then comment on the effect of pooling, ReLUs and performance speed-up providing more details in the appendix.

Is Augmentation still required? Recent works have suggested that binarization is an extreme case of regularization [9, 10, 22]. In light of this, one might wonder whether data augmentation is still required. Our experiments revealed (see Table 6) that in order to accommodate the presence of new poses and/or scale variations, data augmentation is very helpful providing a large increase (4%) in performance.

Layer type	#parameters	PCKh
(Ours, Final) (No Aug.)	6.2M	72.1%
(Ours, Final) + Aug.	6.M	76%

Table 6: The effect of using augmentation when training our binary network in terms of PCKh-based performance on MPII validation set.

The effect of loss. We followed the standard approach for training our binary network to predict a set of heatmaps one for each landmark [29]. To this end, we experimented with two types of losses: the first one is to place a Gaussian around the correct location of each landmark and train using a pixel-wise L2 loss:

$$l = \frac{1}{N} \sum_{n=1}^N \sum_{ij} \left\| \widetilde{M}_n(i, j) - M_n(i, j) \right\|^2, \quad (3)$$

where $\widetilde{M}_n(i, j)$ and $M_n(i, j)$ denote the predicted and the ground truth confidence maps at pixel location (i, j) for the n th landmark, respectively.

However, the gradients generated by this loss are usually small even for the case of real-valued network. Because binarized networks tend to amplify this problem, as an alternatives we also experimented the Sigmoid cross-entropy pixel-wise loss (see eq. 4), typically used for detection tasks:

$$l = \frac{1}{N} \sum_{n=1}^N \sum_{i=1}^W \sum_{j=1}^H [p_{ij}^n \log \hat{p}_{ij}^n + (1-p_{ij}^n) \log(1-\hat{p}_{ij}^n)], \quad (4)$$

where p_{ij}^n represent the ground truth map of the n th landmark at pixel location (i, j) and \hat{p}_{ij}^n is the corresponding sigmoid output at the same location.

We found that the use of the Sigmoid cross-entropy pixel-wise loss increased the gradients by 10-15x (when compared to the L2 loss), offering an 2% improvement (see Table 7), after being trained for the same number of epochs.

Layer type	# parameters	PCKh
(Ours, Final) + L2	6.2M	73.8%
(Ours, Final) + Sigmoid	6.2M	76%

Table 7: The effect of using different losses (Sigmoid vs L2) when training our binary network in terms of PCKh-based performance on MPII validation set.

Pooling type. In line with [25], we found that max-pooling outperforms average pooling: max-pooling results in 4% PCKh-based performance increase on MPII validation set. See supplementary material for more details.

With or without ReLU. In line with [25], we found that by adding a ReLU activation after each convolutional layer performance is increased : we observe a 2% performance improvement on MPII validation set. See supplementary material for more details.

Performance. In line with [25], we observed speedups of up to 3.5x when compared against cuBLAS. We did not conduct experiments on CPUs. However, since we used the same method for binarization as in [25], speed improvements of the order of 58x, are to be expected allowing the system to run in real-time on a CPU using a single core. In terms of memory compression, we can achieve a compression rate of 39x when compared against its single precision counterpart from Torch. See supplementary material for more details.

7. Comparison with state-of-the-art

In this section, we present further experiments illustrating merits and drawbacks of our architecture. An overview of our experiments is as follows:

- Our final system (used here) comprises a single HG network but replaces the original real-valued bottleneck block (used in [23]) with the proposed **binary parallel, multi-scale block** of Fig. 8e trained with the improvements detailed in section 6.
- We compare our method against the current state-of-the-art for the tasks of human pose estimation and 3D face alignment.
- We show that our method achieves competitive results on human pose estimation while being orders of

magnitude more efficient. On 3D face alignment, our method significantly outperforms the current best performing methods offering an improvement of up to 35%.

7.1. Human Pose Estimation

Datasets. We evaluated the proposed block on the challenging MPII [1] dataset. MPII consists of more than 25000 images, containing 40000 subjects in various poses. All samples are annotated with up to 16 points. We used the standard training-validation partition of [3, 23] in which 3000 images are used for validation and the rest for training (29000 images).

We report the performance of (a) the proposed binary block, denoted as [1x, Bi, Ours] in Table 8, (b) the proposed block when implemented and trained with real values (denoted as [1x, Re, Ours]) and finally (c) the real-valued stacked HG network consisting of 8 stacked single real-valued HG networks trained with intermediate supervision, which is currently the best performing method on MPII (denoted as [8x, Re, Bot]) [23].

The results are shown in Table 8. [23] performs better as expected; however it uses 8 HG networks having far more parameters, and also benefiting from training with intermediate supervision. Notably, when a single HG network with the proposed block is trained with real weights, its performance reaches that of [23]. This result clearly illustrates the enhanced learning capacity of the proposed block. We also observe that there is still a gap between the binary and real-valued version of the proposed block indicating that margin for further improvement is possible. Note that since our aim is to consider landmark localization with limited resources, we did not investigate network stacking which dramatically increases the number of parameters and complexity but we leave that for interesting future work.

7.2. Face alignment

Datasets. We evaluated our method on two of the most challenging datasets for large pose 3D face alignment, namely AFLW-PIFA [16] and AFLW2000-3D [35]. The evaluation metric commonly used for these datasets is the Normalized Mean Error (NME) [16].

AFLW-PIFA is a grey-scale subset of AFLW, consisting of 5200 images selected so that there is a balanced number of images for yaw angle in $[0^\circ, 30^\circ]$, $[30^\circ, 60^\circ]$ and $[60^\circ, 90^\circ]$. Following [16], 3901 images were used for training and 1299 for testing. All images were annotated with 34 points from a 3D perspective.

Tables 9 and 10 show our results on AFLW-PIFA. When evaluated on both visible and occluded points, our method improves upon the current best result of [2] by more than

Crit.	[8x, Re, Bot][23]	[1x, Bi, Ours]	[1x, Re, Ours]
Head	97.3	94.7	96.8
Shld	96.0	89.6	93.8
Elbow	90.2	78.8	86.4
Wrist	85.2	71.5	80.3
Hip	89.1	79.1	87.0
Knee	85.1	70.5	80.4
Ankle	82.0	64.0	75.7
PCKh	89.3	78.1	85.5
# par.	25M	6M	6M

Table 8: PCKh-based comparison on MPII validation set. The following notation is used: [#HG networks, Binarized/Real, Block type].

10%. Notably, our method uses a binary network as opposed to real-valued systems proposed in prior work.

AFLW2000-3D is a subset of the AFLW dataset[18] re-annotated by [35] from a 3D perspective with 68 points. We used this dataset only for evaluation. The training was done using the first 40000 images from the 300W-LP [35].

On AFLW2000-3D, the improvement is even larger. See Table 11 and Fig. 10. Our binary method outperforms the current (real-valued) state-of-the-art method of [35] by more than 35%. While our method improves over the entire range of poses, the gain is noticeably higher for large poses ($[60^{\circ} - 90^{\circ}]$) where we outperform [35] by more than 40%.

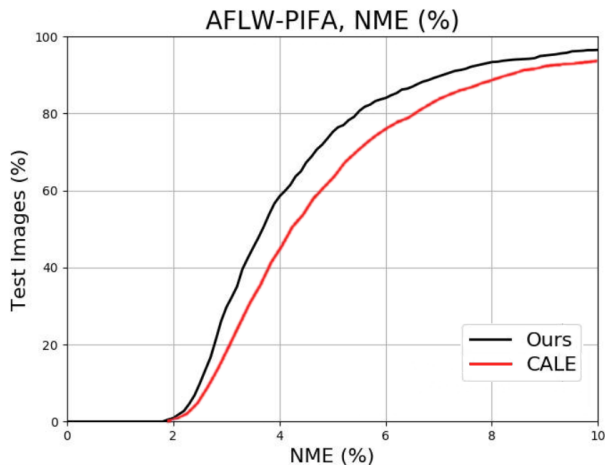


Figure 9: Cumulative error curves on AFLW-PIFA, evaluated on all 34 points, both visible and occluded. CALE denotes the method of [2].

8. Conclusion

In this paper, we proposed a novel block architecture, particularly tailored for binarized CNNs for the tasks

PIFA [16]	RCPR [5]	PAWF [17]	CALE [2]	Ours
8.04	6.26	4.72	2.96	3.02

Table 9: NME-based (%) based comparison on AFLW-PIFA evaluated on visible landmarks only. The results for PIFA, RCPR and PAWF are taken from [17].

CALE [2]	Ours
4.97	4.47

Table 10: NME-based (%) based comparison on AFLW-PIFA evaluated on all 34 points, both visible and occluded.

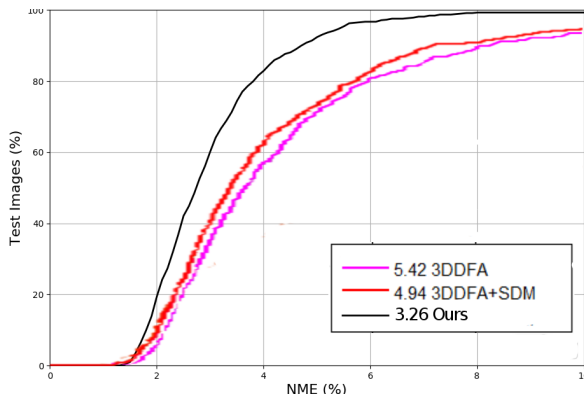


Figure 10: Cumulative error curves on AFLW2000-3D for both visible and occluded points computed on a random subset of 696 images, the absolute yaw angles of which are equally represented in $[0^{\circ}, 30^{\circ}]$, $[30^{\circ}, 60^{\circ}]$, $[60^{\circ}, 90^{\circ}]$ (similar to the experiment reported in [35]). The curves for 3DDFA and SDDFA+SDM are extracted from [35].



(a) Fitting examples produced by our binary network on AFLW2000-3D dataset. Notice that our method copes well with extreme poses and expressions, in various lightning and coloring (both color and grayscale) conditions.



(b) Examples of human poses obtained using our binary network. Observe that our method produces good results for a wide variety of poses and occlusions.

Figure 11: Qualitative results produced by our method on (a) AFLW2000-3D and (b) MPII datasets.

Method	[0,30]	[30,60]	[60,90]	Mean
RCPR(300W) [5]	4.16	9.88	22.58	12.21
RCPR(300W-LP) [5]	4.26	5.96	13.18	7.80
ESR(300W) [6]	4.38	10.47	20.31	11.72
ESR(300W-LP) [6]	4.60	6.70	12.67	7.99
SDM(300W) [33]	3.56	7.08	17.48	9.37
SDM(300W-LP) [33]	3.67	4.94	9.76	6.12
3DDFA [35]	3.78	4.54	7.93	5.42
3DDFA+SDM [35]	3.43	4.24	7.17	4.94
Ours	2.47	3.01	4.31	3.26

Table 11: NME-based (%) based comparison on AFLW2000-3D evaluated on all 68 points, both visible and occluded. The results for RCPR, ESR and SDM are taken from [35].

of human pose estimation and face alignment. During the process, we exhaustively evaluated various design choices, identified performance bottlenecks and proposed solutions. We showed that our hierarchical, parallel and multiscale module enhances representational power, allowing for stronger relations to be learned without excessively increasing the number of network parameters. The proposed architecture is efficient and can run on limited computational resources.

9. Appendix

This Section provides additional details for some of the ablation studies reported in Section 6.

Pooling type. In the context of binary networks, and because the output is restricted to 1 and -1, max-pooling might result in outputs full of 1s only. To limit this effect, we placed the activation function before the convolutional layers as proposed in [12, 25]. Additionally, we opted to

replace max-pooling with average pooling. However, this leads to slightly worse results (see Table 12). In practice, we found that the use of blocks with pre-activation suffices and that the ratio of 1 and -1 is close to 50% even after max-pooling.

Layer type	# parameters	PCKh
(Ours, Final) + Average	6.2M	71.9%
(Ours, Final) + Max	6.2M	76%

Table 12: The effect of using different pooling methods when training our binary network in terms of PCKh-based performance on MPII validation set.

With or without ReLU. Because during the binarization process all ReLU layers are replaced with the Sign function, one might wonder if ReLUs are still useful for the binary case. Our findings are in line with the ones reported in [25]. By adding a ReLU activation after each convolutional layer, we observe a 2% performance improvement (see Table 13), which can be attributed to the added non-linearity, particularly useful for training very deep architectures.

Layer type	#parameters	PCKh
(Ours, Final)	6.2M	76%
(Ours, Final) + ReLU	6.2M	77.8%

Table 13: The effect of using ReLU when training our binary network in terms of PCKh-based performance on MPII validation set.

Performance. In theory, by replacing all floating-point multiplications with bitwise XOR and making use of the SWAR (Single instruction, multiple data within a register) [25, 10], the number of operations can be reduced up to 32x when compared against the multiplication-based convolution.

However, in our tests, we observed speedups of up to 3.5x, when compared against cuBLAS, for matrix multiplications, a result being in accordance with those reported in [10]. As GPUs are already available on mobile devices, we did not conduct experiments on CPUs. However, given the fact that we used the same method for binarization as in [25], similar improvements in terms of speed, of the order of 58x, are to be expected: as the real-valued network takes 0.67 seconds to do a forward pass on a i7-3820 using a single core, a speedup close to x58 will allow the system to run in real-time. Our Torch7 [7] implementation will be made available on our page.

In terms of memory compression, by removing the biases, which have minimum impact (or no impact at all) on performance, and by grouping and storing every 32 weights

in one variable, we can achieve a compression rate of 39x when compared against the single precision counterpart of Torch. See Fig. 12.



Figure 12: Memory compression ratio. By binarizing the weights and removing the biases, we achieve a compression rate of 39x when compared against the single precision model.

References

- [1] M. Andriluka, L. Pishchulin, P. Gehler, and B. Schiele. 2d human pose estimation: New benchmark and state of the art analysis. In *CVPR*, pages 3686–3693, 2014.
- [2] A. Bulat and G. Tzimiropoulos. Convolutional aggregation of local evidence for large pose face alignment. 2016.
- [3] A. Bulat and G. Tzimiropoulos. Human pose estimation via convolutional part heatmap regression. In *ECCV*, pages 717–732. Springer, 2016.
- [4] A. Bulat and G. Tzimiropoulos. Two-stage convolutional part heatmap regression for the 1st 3d face alignment in the wild (3dfaw) challenge. In *ECCV*, pages 616–624. Springer International Publishing, 2016.
- [5] X. P. Burgos-Artizzu, P. Perona, and P. Dollár. Robust face landmark estimation under occlusion. In *ICCV*, pages 1513–1520, 2013.
- [6] X. Cao, Y. Wei, F. Wen, and J. Sun. Face alignment by explicit shape regression. *International Journal of Computer Vision*, 107(2):177–190, 2014.
- [7] R. Collobert, K. Kavukcuoglu, and C. Farabet. Torch7: A matlab-like environment for machine learning. In *NIPS-W*, number EPFL-CONF-192376, 2011.
- [8] M. Courbariaux, Y. Bengio, and J.-P. David. Training deep neural networks with low precision multiplications. *arXiv*, 2014.
- [9] M. Courbariaux, Y. Bengio, and J.-P. David. Binaryconnect: Training deep neural networks with binary weights during propagations. In *NIPS*, pages 3123–3131, 2015.

- [10] M. Courbariaux, I. Hubara, D. Soudry, R. El-Yaniv, and Y. Bengio. Binarized neural networks: Training deep neural networks with weights and activations constrained to+ 1 or-1. *arXiv*, 2016.
- [11] K. He, X. Zhang, S. Ren, and J. Sun. Deep residual learning for image recognition. In *CVPR*, 2016.
- [12] K. He, X. Zhang, S. Ren, and J. Sun. Identity mappings in deep residual networks. In *ECCV*, pages 630–645. Springer, 2016.
- [13] J. L. Holli and J.-N. Hwang. Finite precision error analysis of neural network hardware implementations. *IEEE Transactions on Computers*, 42(3):281–290, 1993.
- [14] E. Insafutdinov, L. Pishchulin, B. Andres, M. Andriluka, and B. Schiele. Deeppercut: A deeper, stronger, and faster multi-person pose estimation model. In *ECCV*, pages 34–50. Springer, 2016.
- [15] S. Ioffe and C. Szegedy. Batch normalization: Accelerating deep network training by reducing internal covariate shift. *arXiv*, 2015.
- [16] A. Jourabloo and X. Liu. Pose-invariant 3d face alignment. In *ICCV*, pages 3694–3702, 2015.
- [17] A. Jourabloo and X. Liu. Large-pose face alignment via cnn-based dense 3d model fitting. In *CVPR*, pages 4188–4196, 2016.
- [18] M. Köstinger, P. Wohlhart, P. M. Roth, and H. Bischof. Annotated facial landmarks in the wild: A large-scale, real-world database for facial landmark localization. In *ICCV-W*, pages 2144–2151. IEEE, 2011.
- [19] A. Krizhevsky and G. Hinton. Learning multiple layers of features from tiny images. 2009.
- [20] D. D. Lin, S. S. Talathi, and V. S. Annapureddy. Fixed point quantization of deep convolutional networks. *arXiv*, 2015.
- [21] J. Long, E. Shelhamer, and T. Darrell. Fully convolutional networks for semantic segmentation. In *CVPR*, pages 3431–3440, 2015.
- [22] P. Merolla, R. Appuswamy, J. Arthur, S. K. Esser, and D. Modha. Deep neural networks are robust to weight binarization and other non-linear distortions. *arXiv*, 2016.
- [23] A. Newell, K. Yang, and J. Deng. Stacked hourglass networks for human pose estimation. In *ECCV*, pages 483–499. Springer, 2016.
- [24] T. Pfister, J. Charles, and A. Zisserman. Flowing convnets for human pose estimation in videos. In *ICCV*, pages 1913–1921, 2015.
- [25] M. Rastegari, V. Ordonez, J. Redmon, and A. Farhadi. Xnet: Imagenet classification using binary convolutional neural networks. In *ECCV*, pages 525–542. Springer, 2016.
- [26] K. Simonyan and A. Zisserman. Very deep convolutional networks for large-scale image recognition. *arXiv*, 2014.
- [27] D. Soudry, I. Hubara, and R. Meir. Expectation backpropagation: Parameter-free training of multilayer neural networks with continuous or discrete weights. In *NIPS*, pages 963–971, 2014.
- [28] C. Szegedy, W. Liu, Y. Jia, P. Sermanet, S. Reed, D. Anguelov, D. Erhan, V. Vanhoucke, and A. Rabinovich. Going deeper with convolutions. In *CVPR*, pages 1–9, 2015.
- [29] J. J. Tompson, A. Jain, Y. LeCun, and C. Bregler. Joint training of a convolutional network and a graphical model for human pose estimation. In *NIPS*, pages 1799–1807, 2014.
- [30] A. Toshev and C. Szegedy. Deeppose: Human pose estimation via deep neural networks. In *CVPR*, pages 1653–1660, 2014.
- [31] S.-E. Wei, V. Ramakrishna, T. Kanade, and Y. Sheikh. Convolutional pose machines. In *CVPR*, pages 4724–4732, 2016.
- [32] S. Xie, R. Girshick, P. Dollár, Z. Tu, and K. He. Aggregated residual transformations for deep neural networks. *arXiv*, 2016.
- [33] X. Xiong and F. De la Torre. Supervised descent method and its applications to face alignment. In *CVPR*, pages 532–539, 2013.
- [34] S. Zagoruyko and N. Komodakis. Wide residual networks. *arXiv*, 2016.
- [35] X. Zhu, Z. Lei, X. Liu, H. Shi, and S. Z. Li. Face alignment across large poses: A 3d solution. In *CVPR*, pages 146–155, 2016.